Dalton Transactions

Cite this: *Dalton Trans.*, 2012, **41**, 5581

www.rsc.org/dalton

PAPER

Controlled synthesis of olive-shaped $Bi_2S_3/BiVO_4$ microspheres through a limited chemical conversion route and enhanced visible-light-responding photocatalytic activity†

De-Kun Ma,* Mei-Li Guan, Sen-Sen Liu, Yan-Qing Zhang, Chang-Wei Zhang, Yu-Xiang He and Shao-Ming Huang*

Received 15th January 2012, Accepted 17th February 2012
DOI: 10.1039/c2dt30099k

Well-defined olive-shaped $Bi_2S_3/BiVO_4$ microspheres were synthesized through a limited chemical conversion route (LCCR), where olive-shaped $BiVO_4$ microspheres and thioacetamide (TAA) were used as precursors and sulfur source, respectively. The as-synthesized products were characterized by X-ray diffraction (XRD), field emission scanning electron microscopy (FE-SEM), high-resolution transmission microscope (HRTEM), X-ray photoelectron spectra (XPS), UV-visible diffuse-reflectance spectroscopy (UV-vis DRS), and photoluminescence (PL) spectra in detail. Compared with pure $BiVO_4$ microspheres and Bi_2S_3 nanorods, the $Bi_2S_3/BiVO_4$ products showed obviously enhanced photocatalytic activity for the degradation of rhodamine B (Rh B) in aqueous solution under visible-light irradiation ($\lambda > 400$ nm). In addition, the $Bi_2S_3/BiVO_4$ composite microspheres showed good visible-light-driven photocatalytic activity for the degradation of refractory oxytetracycline (OTC) as well. On the basis of UV-vis DRS, the calculated energy band positions, and PL spectra, the mechanism of enhanced photocatalytic activity of $Bi_2S_3/BiVO_4$ was proposed. The present study provides a new strategy to design composite materials with enhanced photocatalytic performance.

Introduction

In recent years, visible-light-responding photocatalysts have aroused tremendous interest because of their potential applications in splitting of water, degradation of organic pollutants, and reduction of CO_2 into renewable hydrocarbon fuel.[1–5] Up to now, many efforts have been made to synthesize Bi-based oxide semiconductors such as Bi_2WO_6, $BiVO_4$, $BiFeO_3$, and Bi_2O_3 because of their good photocatalytic activity under visible-light irradiation, which is attributed to the hybridized valence band (VB) of O 2p and Bi 6s which narrows the band gap.[6–10] As a member of Bi-based oxides, $BiVO_4$ has been extensively studied because of its unique properties including ferroelasticity,[11] ionic conductivity,[12] gas sensing,[13] and coloristic properties.[14] Since Kudo and coauthors reported the photocatalytic activity of $BiVO_4$ in 1998,[15] a number of studies have been focused on the controlled synthesis of its monoclinic phase structure,[16] morphology with large surface area,[17] and exposed high-energy facets.[18] However, the photocatalytic activity of the individual $BiVO_4$ is not ideal yet for practical application. Previous studies had showed that composite photocatalysts could extend the spectral responsive range and promote the separation of photoinduced carriers and thus would improve photocatalytic activity of single-component materials dramatically.[19] More recently, we synthesized n–p core–shell $BiVO_4@Bi_2O_3$ microspheres and found that $BiVO_4@Bi_2O_3$ composites showed better photocatalytic activity than the single $BiVO_4$ and Bi_2O_3.[20] However, the introduction of Bi_2O_3 into the composites could only facilitate efficient separation of photogenerated carriers. Therefore, it is highly desirable to develop new $BiVO_4$-based composites, where the combination of a suitable semiconductor with $BiVO_4$ will both benefit efficient separation of photogenerated electrons and holes and large extension of spectral responsive range.

Bi_2S_3 is a direct narrow band-gap semiconductor (~1.3 eV), which has attracted much attention because of its potential applications in many fields such as electrochemical hydrogen storage,[21] hydrogen sensor,[22] X-ray computed tomography imaging,[23] biomolecule detection,[24] and lithium ion battery.[25] Owing to its narrow band-gap, large absorption coefficient, and reasonable incident photon to electron conversion efficiency, Bi_2S_3 is also a promising semiconductor material for the fabrication of photoelectrochemical devices,[26] photodetectors,[27] and photovoltaic cells.[28] Robert *et al.* reported that Bi_2S_3 could be used as an efficient sensitizer to absorb a large part of visible light up to 800 nm.[29] We calculated the energy band positions of Bi_2S_3 and $BiVO_4$ and found that the combination of $BiVO_4$

Nanomaterials and Chemistry Key Laboratory, Wenzhou University, Wenzhou, Zhejiang 325027, P. R. China. E-mail: dkma@wzu.edu.cn, smhuang@wzu.edu.cn

†Electronic supplementary information (ESI) available: The synthetic process, XRD pattern, FE-SEM image of Bi_2S_3 nanorods, UV-vis absorption spectra changes of Rh B aqueous solution in the presence of different products and Rh B concentration changes in different samples. See DOI: 10.1039/c2dt30099k

with Bi_2S_3 was helpful to separate photogenerated carriers. Therefore, the photocatalytic activity of $BiVO_4$ will be enhanced if we can fabricate $Bi_2S_3/BiVO_4$ composite materials with a good heterojunction. However, up to now, to the best of our knowledge, $Bi_2S_3/BiVO_4$ composite photocatalysts have never been reported.

Compounds with high-solubility products can be converted into other compounds with low-solubility products under the driving force of solubility difference in solution. Bi_2S_3 has very low solubility products ($K_{sp} = 1 \times 10^{-97}$). Therefore $BiVO_4$ can easily convert into Bi_2S_3 when anion exchange takes place with S^{2-} ions in solution under certain conditions. If this kind of anion exchange is controlled at a limited level, $BiVO_4$ will be partly transformed into Bi_2S_3 and thus $Bi_2S_3/BiVO_4$ composite materials will be produced. Here we define this method as a limited chemical conversion route (LCCR). In this study, we synthesized olive-shaped $Bi_2S_3/BiVO_4$ composite microspheres through the LCCR, where olive-shaped $BiVO_4$ microspheres and thioacetamide (TAA) were used as precursors and sulfur source, respectively. Furthermore, the visible-light-driven photocatalytic properties and mechanism of $Bi_2S_3/BiVO_4$ composite microspheres were studied as well.

Experimental section

Synthesis of $Bi_2S_3/BiVO_4$ microspheres

The synthesis of olive-shaped $BiVO_4$ microspheres adopted our previous method.[20] In a typical procedure for the synthesis of $Bi_2S_3/BiVO_4$, 0.25 mmol of $BiVO_4$ was dispersed in 40 mL of ultrapure water under vigorous stirring. Then a certain amount of TAA was added into the solution. After 5 min stirring, the solution was put into a Teflon® lined stainless steel autoclave of 50 mL capability and heated at 120 °C for 8 h. After the autoclave was cooled to room temperature, the products were separated centrifugally and washed three times with ultrapure water and absolute ethanol. Then the products were dried under vacuum at 60 °C for 4 h. Before characterization and photocatalytic property study, the products were further heated at 200 °C for 30 min in order to improve their crystallinity and remove physically absorbed water molecules.

Characterization

Powder X-ray diffraction (XRD) was performed on a Bruker D8 Advance X-ray diffractometer using Cu Kα radiation (λ = 0.15418 nm) at a scanning rate of 8° min^{-1} in the 2θ range from 10 to 70°. Field emission scanning electron microscopy (FE-SEM) images were taken on a Nova NanoSEM 200 scanning electron microscope (FEI Inc.). High-resolution transmission microscope (HRTEM) images were performed on a JEOL JEM 2010 high-resolution transmission electron microscope, using an accelerating voltage of 200 kV. X-ray photoelectron spectroscopy (XPS) measurements were carried out with a Thermo ESCALAB 250 X-ray photoelectron spectrometer with an excitation source of Al Kα radiation (λ = 1253.6 eV). The optical diffuse-reflectance spectra were recorded on a Lambda 950 (Perkin Elmer) using $BaSO_4$ as a reference. The photoluminescence spectra were recorded on a Fluoromax-4 spectrofluorometer (HORIBA Jobin Yvon Inc.) equipped with a 150 W xenon lamp as the excitation source. All of the measurements were performed at room temperature.

Photocatalytic properties

The photocatalytic activity of $Bi_2S_3/BiVO_4$ was evaluated by degradation of Rh B under visible-light irradiation from 500 W Xe light (CHF-XM500, purchased from Beijing Trusttech Co., Ltd) equipped with a 400 nm cutoff filter. In a typical process, 100 mg of photocatalysts were added to 100 mL of a Rh B solution (10^{-5} mol L^{-1}). Before illumination, the solution was magnetically stirred in the dark for 24 h to ensure the establishment of an adsorption–desorption equilibrium between the photocatalysts and Rh B. After that, the solution was exposed to visible-light irradiation under magnetic stirring. At given time intervals, 3 mL aliquots were sampled and centrifuged to remove the photocatalyst particles. Then, the filtrates were analyzed by recording variations of the absorption band maximum (553 nm) in the UV-vis spectra of Rh B by using a Shimadzu UV2501PC spectrophotometer. The studies of photocatalytic activities for other samples adopted the same measurement process. As to the degradation study of oxytetracycline (OTC), keeping other conditions unchanged, the initial concentration of OTC solution was 0.2 mg mL^{-1}. After visible light irradiation of different period time, the centrifugated solution was analyzed by recording variations of the absorption band maximum (268 nm) in the UV-vis spectra of OTC by using a Shimadzu UV2501PC spectrophotometer.

Results and discussion

Fig. 1 presents XRD patterns of the products synthesized with different amounts of TAA. It can be seen from Fig. 1a that all reflection peaks of the products can be indexed to a monoclinic scheelite structure of $BiVO_4$ (JCPDS No. 75-2480) when 0.1 mmol of TAA was used. No obvious reflection peaks from Bi_2S_3 can be observed. Interestingly, keeping other synthetic conditions unchanged, as shown in Fig. 1b, the resultant

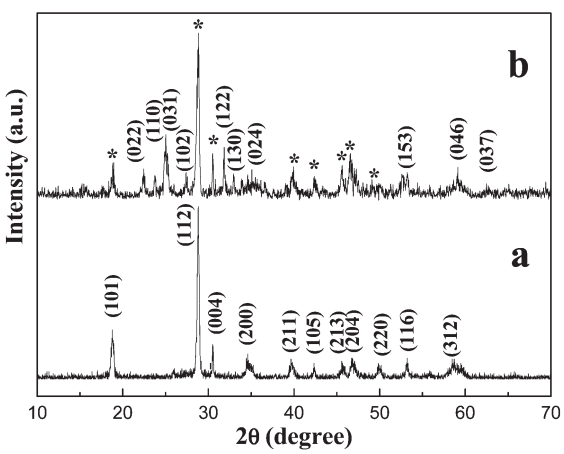

Fig. 1 XRD patterns of the products synthesized with different amounts of TAA: (a) 0.1 mmol and (b) 5 mmol.

products include both reflection peaks of $BiVO_4$ (marked with asterisks) and Bi_2S_3 (JCPDS No. 84-0279) when the amount of TAA was increased to 5 mmol. It means that $BiVO_4$ can be converted into Bi_2S_3 thermodynamically under the present synthetic conditions. According to a previous report,[30] TAA could decompose into S^{2-} ions and other byproducts at 50 °C in aqueous solution. Only when the concentration of Bi^{3+} ions from the dissociation of $BiVO_4$ microspheres and that of S^{2-} ions in solution reaches solubility products will Bi_2S_3 be formed. Therefore, if more TAA was used more Bi_2S_3 would be produced.

In order to confirm the products synthesized with 0.1 mmol of TAA containing both Bi_2S_3 and $BiVO_4$, XPS analyses were carried out. Fig. 2a shows a typical wide-scan XPS spectrum of the products, in which all peaks can be assigned to Bi, V, O, S, and C elements. The binding energy of the C 1s transition at 284.8 eV was used as a reference to calibrate the binding energies of other elements. High-resolution XPS gives the valence state and coordination information of the as-synthesized products. Fig. 2b shows high-resolution XPS spectra of Bi 4f and S 2p of the products. The two strong wide peaks at 164.6 and 159.3 eV can be well fitted into five perfect peaks. The peaks with binding energies of 159.3 and 164.6 eV correspond to Bi $4f_{7/2}$ and Bi $4f_{5/2}$ in $BiVO_4$,[31] respectively. The peaks at 157.2 and 162.6 eV can be attributed to the binding energies of Bi $4f_{7/2}$ and Bi $4f_{5/2}$ in Bi_2S_3,[32] respectively. The peak at 160.4 eV can be assigned to the binding energy of the S 2p transition.[33] The V 2p core level spectrum (Fig. 2c) reveals that the observed values (516.8 and 524.4 eV) of the binding energies for V 2p are in agreement with previous report on V^{5+} in $BiVO_4$.[34] Consequently, the XPS results indicate that the products consist of Bi_2S_3 and $BiVO_4$ with no obvious residual impurities.

According to elemental analysis of S, the amounts of Bi_2S_3 in the products respectively obtained with 0.1 and 5 mmol of TAA were *ca.* 2.4% and 66.7%. This result further showed that only a limited $BiVO_4$ could be converted into Bi_2S_3 under the current synthetic conditions, though excess TAA was used.

Fig. 3 represents FE-SEM images of $BiVO_4$ precursors and the products synthesized with 0.1 mmol of TAA. Compared with $BiVO_4$ precursors (Fig. 3a), the whole morphology of the products obtained with 0.1 mmol of TAA shows no obvious change (Fig. 3b), suggesting that Bi_2S_3 derived from a LCCR can combine well with $BiVO_4$. HRTEM was further used to identify the elaborate structure of the composite microspheres. As can be seen from the magnified TEM image of a typical single microsphere (Fig. 3c), some flake-like substances were grown on the surfaces of olive-shaped $BiVO_4$ microspheres. HRTEM image recorded on the rim of the flake was shown in Fig. 3d. The spacings of the adjacent lattice planes are *ca.* 7.93 and 3.55 Å, which are consistent with the interplanar spacings of (011) and (111) planes of orthogonal Bi_2S_3, respectively. From the results of HRTEM, it can confirm that the obtained products are Bi_2S_3/$BiVO_4$ microspheres. However, many short Bi_2S_3 nanorods would grow on the surfaces of $BiVO_4$ microspheres when 5 mmol of TAA was used (see ESI, Fig. S1†). It can be understood as follows. When 0.1 mmol of TAA was used, only a few Bi_2S_3 crystal nuclei were formed by a LCCR and thus they were inclined to scatter on the surfaces of $BiVO_4$ microspheres in the form of tiny flakes. With the amount of TAA increasing to 5 mmol, large numbers of Bi_2S_3 crystal nuclei would be formed and they could be used as stock for anisotropic growth of Bi_2S_3 into nanorods. For the sake of concision, Bi_2S_3/$BiVO_4$ composite microspheres obtained with 0.1 mmol of TAA was chosen as a candidate for subsequent study.

Fig. 4 describes UV-visible diffuse-reflectance spectroscopy (UV-vis DRS) of $BiVO_4$ precursors, Bi_2S_3 nanorods, and Bi_2S_3/$BiVO_4$ composites obtained with 0.1 mmol of TTA. Here, Bi_2S_3 nanorods were obtained by a similar hydrothermal route at 120 °C for 8 h (See ESI†). As can be seen from Fig. 4a and 4b, the ability of light absorption of $BiVO_4$ is enhanced greatly after Bi_2S_3 was introduced. This should be attributed to the small band gap and large absorption coefficient of Bi_2S_3. Bi_2S_3 has strong absorption in nearly all of the visible light range (Fig. 4c). According to the present results, the light absorption spectrum of the composite semiconductor Bi_2S_3/$BiVO_4$ can be extended into larger range even at lower content of Bi_2S_3.

Whether composite semiconductors are suitable for efficient separation of photogenerated carriers is closely related to their

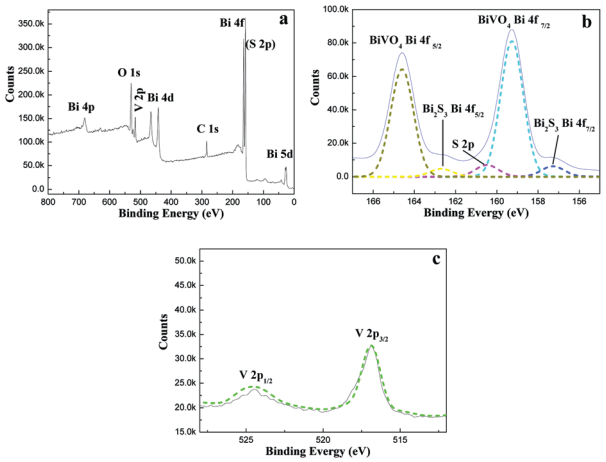

Fig. 2 Typical XPS spectra of the products synthesized with 0.1 mmol of TAA: wide-scan spectrum (a) and high-resolution spectra of the core levels of Bi 4f and S 2p (b) and V 2p (c). The fitted curves were plotted with short dashes.

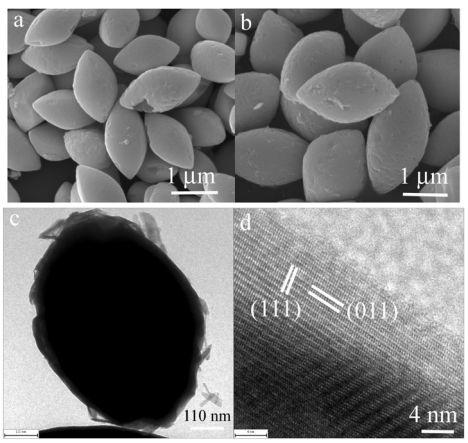

Fig. 3 FE-SEM images of (a) $BiVO_4$ precursors, (b) the products synthesized with 0.1 mmol of TAA, (c) TEM image of an individual Bi_2S_3/$BiVO_4$ composite microsphere, and (d) HRTEM image recorded on the rim of the flake.

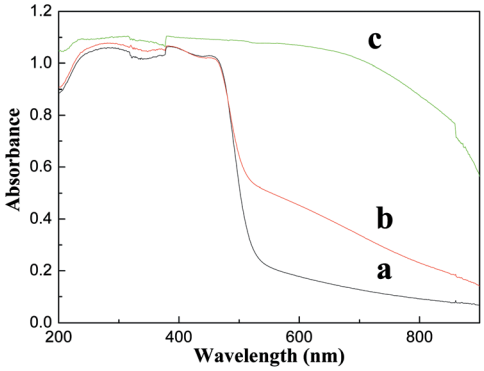

Fig. 4 UV-vis DRS spectra of $BiVO_4$ precursors (a), $Bi_2S_3/BiVO_4$ composites obtained with 0.1 mmol of TAA (b), and Bi_2S_3 nanorods (c).

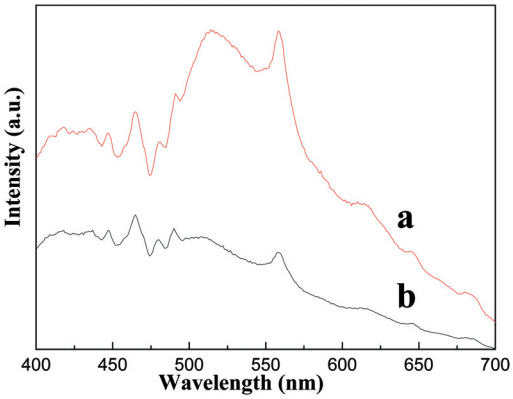

Fig. 5 PL emission spectra of pure $BiVO_4$ (a) and $Bi_2S_3/BiVO_4$ composites (b) excited at 320 nm at room temperature.

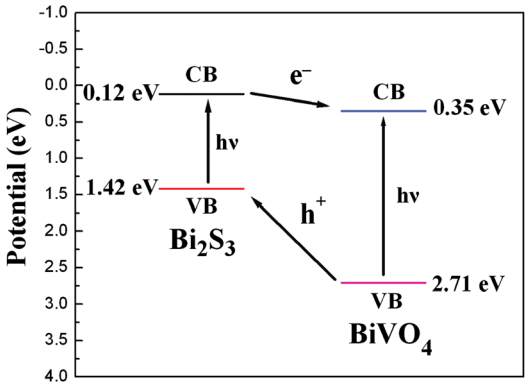

Scheme 1 Diagram for energy band levels of $Bi_2S_3/BiVO_4$ composites and the possible charge separation process.

band-edge positions. The VB edge of a semiconductor at the point of zero charge can be calculated by the empirical equation $E_{VB} = X - E^e + 0.5E_g$,[20] where E_{VB} is the valence band-edge potential, X is the electronegativity of the semiconductor, expressed as the geometric mean of the absolute electronegativity of the constituent atoms, E^e is the energy of free electrons on the hydrogen scale (about 4.5 eV), E_g is the band-gap energy of the semiconductor, and E_{CB} can be determined by $E_{CB} = E_{VB} - E_g$. The X values for $BiVO_4$ and Bi_2S_3 are *ca.* 6.04 and 5.95 eV. The band-gap energies of $BiVO_4$ and Bi_2S_3 are 2.36 and 1.3 eV, respectively. Given the equation above, the top of the valence band and the bottom of the conduction band of $BiVO_4$ and Bi_2S_3 are calculated to be 0.35, 2.71 eV and 0.12, 1.42 eV, respectively. According to the above results, Scheme 1 was proposed to illustrate the energy band levels of $Bi_2S_3/BiVO_4$ and the possible charge-separation process. Under visible-light irradiation, both Bi_2S_3 and $BiVO_4$ are easily excited and corresponding photoelectrons and holes are generated. Photogenerated electrons in Bi_2S_3 are transferred to the CB of $BiVO_4$ because its CB is positioned higher than that of $BiVO_4$. Holes formed in $BiVO_4$ will be migrated to VB of Bi_2S_3 because its VB is more positive than that of Bi_2S_3. In such a way, the photoinduced electrons and holes can be efficiently separated.

Photoluminescence (PL) spectra are a facile technique to survey the separation efficiency of the photogenerated carriers. The higher the PL intensity, the bigger probability of charge

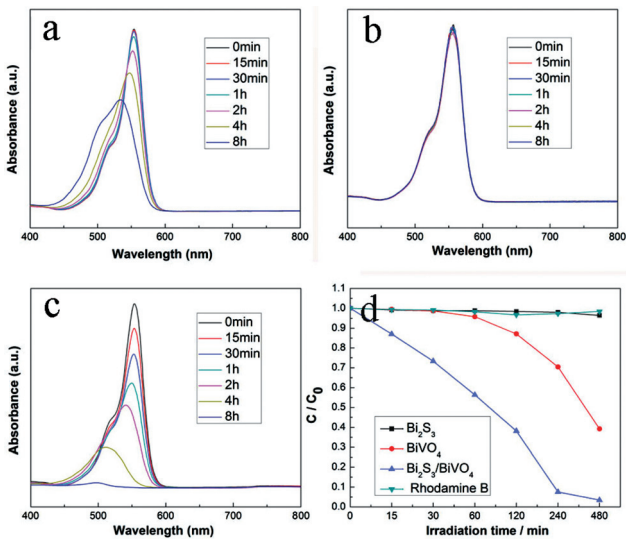

Fig. 6 UV-vis absorption spectra changes of Rh B aqueous solution in the presence of pure $BiVO_4$ (a), Bi_2S_3 nanorods (b), and the products synthesized with 0.1 mmol of TAA (c) as a function of irradiation time. Rh B concentration changes over no catalyst, Bi_2S_3, $BiVO_4$, and $Bi_2S_3/BiVO_4$, respectively (d).

carriers recombination. The room temperature PL emission spectra (excited at 320 nm) of pure $BiVO_4$ and $Bi_2S_3/BiVO_4$ composites are shown in Fig. 5. It can be seen that pure $BiVO_4$ shows a wide emission peak centered at 550 nm, which is similar to a previous report.[35] The luminescence of $BiVO_4$ is considered to come from the recombination of the hole formed in the O 2p band and the electron in the V 3d band. It was found that PL emission intensity of $Bi_2S_3/BiVO_4$ composites was obviously weakened compared with that of pure $BiVO_4$. This result shows that the recombination of photoinduced carriers between O 2p and V 3d is inhibited by a small quantity of Bi_2S_3 existing in composites. In other words, the combination of $BiVO_4$ and Bi_2S_3 is helpful to separate photogenerated carriers.

The photocatalytic activities of $Bi_2S_3/BiVO_4$ composites were evaluated by decomposing Rh B dye in water under visible-light irradiation ($\lambda > 400$ nm). Parts a–c of Fig. 6 shows the temporal evolution of the UV-vis absorption spectra of Rh B on pure

$BiVO_4$, Bi_2S_3 nanorods, and $Bi_2S_3/BiVO_4$ composite microspheres. As can seen from the above three spectra, absorbance of Rh B in both $BiVO_4$ and $Bi_2S_3/BiVO_4$ suspensions gradually decreased during the photodegradation process. Additionally, the major absorption peak corresponding to Rh B was shifted from 553 to shorter wavelength step by step, indicating the removal of ethyl groups one by one, which was in agreement with the literature.[36] However, absorbance of Rh B in Bi_2S_3 nanorods suspension is hardly changed. This result shows that Bi_2S_3 has lower photocatalytic activity under visible-light irradiation, which is consistent with a previous report.[37] The plots for the concentration changes of Rh B determined from its characteristic absorption peak (at 553 nm) over no catalyst, $BiVO_4$, Bi_2S_3, and $Bi_2S_3/BiVO_4$ composites are shown in Fig. 6d. It can be seen that Rh B has negligible degradation under visible-light irradiation without catalysts, indicating that Rh B is a stable molecule and the photolysis can be ignored. $Bi_2S_3/BiVO_4$ composite microspheres show higher photocatalytic activities than individual $BiVO_4$ and Bi_2S_3 under identical experimental conditions. As discussed above, the combination of $BiVO_4$ and Bi_2S_3 both extends spectral responsive range and facilitates the efficient separation of photogenerated carriers, which can be considered as main reasons for the enhancement of $BiVO_4$ photocatalytic activities. It should be pointed out that the amount of Bi_2S_3 has obvious influence on the photocatalytic activities in the present composite material system. When 0.05 and 0.5 mmol of TAA were respectively used, the photocatalytic activities of both the resultant products were inferior to the products synthesized with 0.1 mmol of TAA (See Fig. S4a–c†). Therefore we believe that the photocatalytic activities of $Bi_2S_3/BiVO_4$ composite photocatalysts will be further improved by delicate adjustment of the amount of Bi_2S_3. The work is in progress.

As a kind of antibiotic, OTC exhibits broad-spectrum antimicrobial activity against a variety of disease-producing bacteria. It has been widely used in animal feed as growth promoters, antibacterial agents in livestock production, aquaculture for therapeutic and prophylactic purposes.[38] However, every coin has its two sides. The abuse of OTC has aroused environmental and ecological concerns.[39] The conventional method is hard to degrade refractory oxytetracycline.[40] Photocatalysis, a kind of advanced oxidation technique, using "green" solar light, can be used to efficiently degrade various organic pollutants. However, up to now, visible-light-driven photocatalytic degradation of OTC has never been reported. On the other hand, OTC has no absorption in the visible-light region. The selection of OTC can further confirm that the degradation of Rh B comes mainly from the photocatalytic process of $Bi_2S_3/BiVO_4$ composite microspheres not the photosensitized one. Fig. 7 shows the temporal UV-vis spectral changes of OTC aqueous solution in the presence of $Bi_2S_3/BiVO_4$ composite microspheres during the photocatalytic degradation process. It can be seen that the main absorbance maximized at *ca.* 268 nm obviously decreased with irradiation time under visible light irradiation ($\lambda > 400$ nm). After 16 h of irradiation, 67% of OTC was degraded. Control experiments demonstrated that visible-light photolysis of OTC (without any catalyst) was very slow and almost no OTC molecules were decomposed during 16 h of irradiation (data not shown here), signifying that the $Bi_2S_3/BiVO_4$ composite microspheres exhibited good photocatalytic activity.

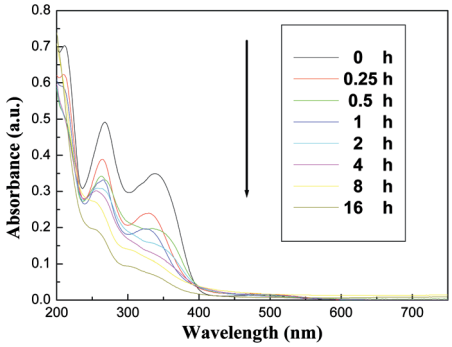

Fig. 7 UV-vis spectroscopic changes of OTC solution in the presence of $Bi_2S_3/BiVO_4$ composite microspheres *vs.* visible-light irradiation time.

Conclusions

In summary, olive-shaped $Bi_2S_3/BiVO_4$ composite microspheres have been successfully synthesized by a LCCR, employing olive-shaped $BiVO_4$ as precursors and TAA as sulfur source. The present method, LCCR, can be extended to synthesize other composite materials in solution phase, where there are obvious solubility differences between different components. The UV-vis DRS, the theoretical calculation on band-edge potential of $BiVO_4$ and Bi_2S_3, PL spectra, and photocatalytic properties studies showed that the combination of $BiVO_4$ and Bi_2S_3 could extend the spectral responsive range of $BiVO_4$ and promote the transfer of photogenerated carriers, thus leading to enhanced photocatalytic activities. Good photocatalytic activity of $Bi_2S_3/BiVO_4$ composite microspheres suggests they are new types of visible-light-driven photocatalysts for environmental remediation.

Acknowledgements

The authors would like to express appreciation for partial financial support from NSFC (51002107), NSFZJ (Y4090118, R4090137), NSFC for Distinguished Young Scholars (51025207), ZJED Innovative Team for S. Huang, and Research Project of College Student Innovative Team of Zhejiang Province (2010R424062).

Notes and references

1 Z. G. Zou, J. H. Ye, K. Sayama and H. Arakawa, *Nature*, 2001, **414**, 625.
2 K. Maeda, K. Teramura, D. L. Lu, T. Takata, N. Saito, Y. Inoue and K. Domen, *Nature*, 2006, **440**, 295.
3 X. C. Wang, K. Maeda, A. Thomas, K. Takanabe, G. Xin, J. M. Carlsson, K. Domen and M. Antonietti, *Nat. Mater.*, 2009, **8**, 76.
4 Z. G. Yi, J. H. Ye, N. Kikugawa, T. Kako, S. X. Ouyang, H. Stuart-Williams, H. Yang, J. Y. Cao, W. J. Luo, Z. S. Li, Y. Liu and R. L. Withers, *Nat. Mater.*, 2010, **9**, 559.
5 L. Cao, S. Sahu, P. Anilkumar, C. E. Bunker, J. Xu, K. A. S. Fernando, P. Wang, E. A. Guliants, K. N. Tackett, II and Y. P. Sun, *J. Am. Chem. Soc.*, 2011, **133**, 4754.
6 D. K. Ma, S. M. Huang, W. X. Chen, S. W. Hu, F. F. Shi and K. L. Fan, *J. Phys. Chem. C*, 2009, **113**, 4369.
7 L. Zhou, W. Z. Wang, S. W. Liu, L. S. Zhang, H. L. Xu and W. Zhu, *J. Mol. Catal. A*, 2006, **252**, 120.
8 F. Gao, X. Y. Chen, K. B. Yin, S. Dong, Z. F. Ren, F. Yuan, T. Yu, Z. G. Zou and J. M. Liu, *Adv. Mater.*, 2007, **19**, 2889.
9 L. Zhou, W. Z. Wang, H. L. Xu, S. M. Sun and M. Shang, *Chem.–Eur. J.*, 2009, **15**, 1776.

10 J. W. Tan, Z. G. Zou and J. H. Ye, *J. Phys. Chem. C*, 2007, **111**, 12779.
11 W. I. F. David and I. G. Wood, *J. Phys. C: Solid State Phys.*, 1983, **16**, 5149.
12 K. Hirota, G. Komatsu, M. Yamashita, H. Takemura and O. Yamaguchi, *Mater. Res. Bull.*, 1992, **27**, 823.
13 Y. Zhao, Y. Xie, X. Zhu, S. Yan and S. X. Wang, *Chem.–Eur. J.*, 2008, **14**, 1601.
14 L. Zhang, D. R. Chen and X. L. Jiao, *J. Phys. Chem. B*, 2006, **110**, 2668.
15 A. Kudo, K. Ueda, H. Kato and I. Mikami, *Catal. Lett.*, 1998, **53**, 229.
16 X. Zhang, Z. H. Ai, F. L. Jia, L. Z. Zhang, X. X. Fan and Z. G. Zou, *Mater. Chem. Phys.*, 2007, **103**, 162.
17 G. S. Li, D. Q. Zhang and J. C. Yu, *Chem. Mater.*, 2008, **20**, 3983.
18 G. C. Xi and J. H. Ye, *Chem. Commun.*, 2010, **46**, 1893.
19 X. B. Chen, S. H. Shen, L. J. Guo and S. S. Mao, *Chem. Rev.*, 2010, **110**, 6503.
20 M. L. Guan, D. K. Ma, S. W. Hu, Y. J. Chen and S. M. Huang, *Inorg. Chem.*, 2011, **50**, 800.
21 B. Zhang, X. C. Ye, W. Y. Hou, Y. Zhao and Y. Xie, *J. Phys. Chem. B*, 2006, **110**, 8978.
22 K. Yao, W. W. Gong, Y. F. Hu, X. L. Liang, Q. Chen and L. M. Peng, *J. Phys. Chem. C*, 2008, **112**, 8721.
23 O. Rabin, J. M. Perez, J. Grimm, G. Wojtkiewicz and R. Weissleder, *Nat. Mater.*, 2006, **5**, 118.
24 L. Cademartiri, F. Scotognella, P. G. O'Brien, B. V. Lotsch, J. Thomson, S. Petrov, N. P. Kherani and G. A. Ozin, *Nano Lett.*, 2009, **9**, 1482.
25 H. Y. Zhou, S. L. Xiong, L. Z. Wei, B. J. Xi, Y. C. Zhu and Y. T. Qian, *Cryst. Growth Des.*, 2009, **9**, 3862.
26 A. Tahir, M. A. Ehsan, M. Mazhar, K. G. Upul Wijayantha, M. Zeller and A. D. Hunter, *Chem. Mater.*, 2010, **22**, 5084.
27 G. Konstantaos, L. Levina, J. Tang and E. H. Sargent, *Nano Lett.*, 2008, **8**, 4002.
28 B. Miller and A. Heller, *Nature*, 1976, **262**, 680.
29 Y. Bessekhouad, D. Robert and J. V. Weber, *J. Photochem. Photobiol., A*, 2004, **163**, 569.
30 K. Yamaguchi, T. Yoshida, D. Lincot and H. Minoura, *J. Phys. Chem. B*, 2003, **107**, 387.
31 M. C. Long, W. M. Cai, J. Cai, B. X. Zhou, X. Y. Chai and Y. H. Wu, *J. Phys. Chem. B*, 2006, **110**, 20211.
32 Z. Chen and M. H. Cao, *Mater. Res. Bull.*, 2011, **46**, 555.
33 L. Tian and H. Y. Tan, *Cryst. Growth Des.*, 2008, **8**, 734.
34 N. Myung, S. Ham, S. Choi, W. G. Kim, Y. J. Jeon, K. J. Paeng, W. Chanmanee, N. R. Tacconi and K. Rajeshwar, *J. Phys. Chem. C*, 2011, **115**, 7793.
35 C. L. Yu, K. Yang, J. C. Yu, F. F. Cao, X. Li and X. C. Zhou, *J. Alloys Compd.*, 2011, **509**, 4547.
36 W. Zhao, C. Chen, X. Li and J. C. Zhao, *J. Phys. Chem. B*, 2002, **106**, 5022.
37 Y. Bessekhouad, D. Robert and J. V. Weber, *J. Photochem. Photobiol., A*, 2004, **163**, 569.
38 P. Kulshrestha, R. F. Giese and D. S. Aga, *Environ. Sci. Technol.*, 2004, **38**, 4097.
39 P. L. Hayes, J. M. Gibbs-Davis, M. J. Musorrafiti, A. L. Mifflin, K. A. Scheidt and F. M. Geiger, *J. Phys. Chem. C*, 2007, **111**, 8796.
40 M. Ö. Uslu and I. A. Balcioğlu, *J. Agric. Food Chem.*, 2009, **57**, 11284.

